



Cite this: *Dalton Trans.*, 2014, **43**, 14680

Synthesis, spectroscopic and electrochemical studies of phosphoryl and carbomethoxyphenyl substituted corroles, and their anion detection properties†

Pinky Yadav and Muniappan Sankar*

The synthesis, electrochemical studies and anion detection properties of triphosphoryl (**2**) and triester corroles (**3**) are reported and compared with triphenylcorrole (**1**). These corroles exhibited typical acid–base binding behaviour in CH₃CN and were converted to monoprotinated and dianionic species, respectively. **2** has shown a ~30 fold lower K_{eq} value for monoprotination than that of **1** in a TFA–CH₃CN medium. The detection ability of these corroles was also tested in acetonitrile towards various anions. The observed spectral changes in free-base corroles (**1–3**) are due to anion-induced deprotonation rather than the hydrogen bonding interaction between the imino protons of the corrole moiety with anions. **2** and **3** have shown higher equilibrium constants with F[−] ions (4.7×10^3 fold higher for **2** and 9.7×10^3 fold higher for **3**) as compared to **1** and are able to detect 0.06 μM of F[−] ions. The Cu(III) and Ag(III) complexes of **2** and **3** exhibited an anodic shift of ~250 mV in first ring oxidation and ~100–150 mV in metal centred reduction as compared to the Cu(III) and Ag(III) complexes of **1**. The anodic shift in the redox potentials, lower protonation constants and lower detection limit of anions have been explained in terms of the electron-withdrawing nature of the diethylphosphite and carbomethoxy substituents at the *meso*-phenyl positions of the corrole ring.

Received 20th June 2014,
Accepted 4th August 2014

DOI: 10.1039/c4dt01853b

www.rsc.org/dalton

Introduction

Johnson and Kay discovered the corrole macrocycle as a by-product during the synthesis of vitamin B₁₂ in the late 1960s.¹ Corroles were widely explored after the successful synthesis of triaryl corroles by Paolesse *et al.* and Gross *et al.* at the same time.^{2,3} After that, the synthetic methodology about corroles has improved significantly.⁴ The development of corroles has led to the new version of a fully aromatic corrin ring.^{5–10} The direct pyrrole–pyrrole linkage is responsible for their unique physico-chemical properties. Unlike porphyrins, corroles can stabilize the higher oxidation state of metal centers.^{10,11} Furthermore, low valent metal complexes are extremely reactive when chelated by corroles and the opposite holds true for their high valent counter parts. The corroles and their metal complexes have been extensively utilized in the areas of catalysis,^{12–18} sensors,^{19,20} artificial light-harvesting antennas,²¹

dye sensitized solar cells,^{22,23} medicinal chemistry²⁴, and non-linear optical materials (NLO).^{25–27}

Sulphonic, phosphonic and carboxylic acid substituted porphyrins show good efficiency in dye-sensitized solar cells. Recently, β-substituted carboxy²³ or sulphonic acid²² substituted corroles were used in dye-sensitized solar cells. Phosphorylporphyrins have been reported as structural building blocks for supramolecular assemblies.^{28–31} Porphyrins substituted with diethoxyphosphoryl groups at the *meso*-position of the ring or the *para*-position of the *meso*-phenyl ring show aggregation tendencies in solution. Corroles exhibit interesting physical and chemical properties when compared with porphyrins because of their lower symmetry (C_{2v}).

Corroles can be deprotonated easily due to their high NH-acidity as compared to porphyrins, which require vigorous conditions. Corrole forms a stable dianion after abstraction of two protons by a strong base such as TBAOH, which shows typical characteristics of aromatic compounds.³² The UV-Visible spectrum obtained after monoprotination of the macrocycle shows aromatic nature, whereas in concentrated acids, it loses the aromatic nature since the second proton is attached to the *meso*-position of the macrocycle.^{32–37}

In recent years, several studies have been carried out in order to explore different fluorescent materials for the develop-

Department of Chemistry, Indian Institute of Technology Roorkee, Roorkee – 247667, India. E-mail: sankafcy@iitr.ac.in

†Electronic supplementary information (ESI) available: Figures of optical absorption and emission spectra, ¹H NMR spectra, MALDI-TOF mass spectra, UV-Visible spectral titrations for the protonation, deprotonation and anion binding studies and cyclic voltammograms of free-base corroles. See DOI: 10.1039/c4dt01853b

ment of chemical sensors. In general, corroles show intense absorption and emission in the visible region, good photostability in various solvents and high NH-acidity. All these characteristics of corroles are useful and quite interesting in anion sensor¹⁹ and pH sensor³⁹ applications. Anion sensing plays an important role in environmental science and biochemistry. As an example, the F⁻ ion is an important anion in the human body, which prevents dental caries and maintains solidity of bones. Anion sensing based on porphyrin and corrole receptors are of current interest.^{19,38,40–42} Recently, Cavaleiro and co-workers have studied the anion sensing properties using the free-base of 5,10,15-tris(pentafluorophenyl)-corrole (H₃TF₅PCor) and its derivatives.²⁰ In this paper, we report the synthesis, electronic spectral, electrochemical redox properties and anion detection abilities of corroles bearing diethoxyphosphoryl and carbomethoxy groups at the *para*-position of the *meso*-phenyl ring. To the best of our knowledge, this is the first report on corroles, which describes the correct mechanism of anion detection (anion induced deprotonation rather than H-bonding) and shows the lower detection limit towards basic anions such as fluoride, acetate and dihydrogenphosphate ions.

Experimental section

Chemicals

4-Bromobenzaldehyde, 4-carbomethoxybenzaldehyde and Pd(PPh₃)₄ were purchased from Alfa Aesar and used as received. Et₃N, hexane and CH₃CN were dried and distilled over CaH₂. CHCl₃ and toluene were dried and distilled over P₂O₅. 5,10,15-Triphenylcorrole (**1**) and 5,10,15-tris(4'-carbomethoxyphenyl)corrole (**3**) were synthesized according to a literature procedure.⁴ Tetrabutylammonium salts (TBAX, X = F, Cl, Br, I, CH₃COO, H₂PO₄, HSO₄, PF₆ and ClO₄) were used as received from Alfa Aesar. We have calculated the limit of detection (LOD) and the limit of quantification (LOQ) for anions by **2** and **3** using the formula, LOD = 3.3 SD/S and LOQ = 10 SD/S, where SD stands for standard deviation of blank, S stands for slope.⁴³

Instrumentation

UV-Visible and fluorescence spectra were recorded using a Cary 100 spectrophotometer and Hitachi F-4600 spectrofluorometer, respectively. All ¹H NMR measurements were performed using a Bruker AVANCE 500 MHz spectrometer in CDCl₃. MALDI-TOF mass spectra were measured using a Bruker UltrafleXtreme-TN MALDI-TOF/TOF spectrometer using dithranol as a matrix. The ESI Mass spectrum of **2** was recorded using a Bruker daltonics-microTOF instrument in negative ion mode and elemental analyses were carried out on a Elementar vario EL III instrument. Electrochemical measurements were carried out with a BAS Epsilon electrochemical workstation. A three-electrode system, consisting of a GC Working electrode, Ag/AgCl reference electrode and a Pt-wire counter electrode, was used. The concentration of all corroles

employed was ~1 mM. All measurements were performed in triply distilled CH₂Cl₂, which was purged with Ar gas using 0.1 M TBAP as the supporting electrolyte. Protonation, deprotonation and anion induced deprotonation of corrole **1–3** were carried out in CH₃CN at room temperature. The equilibrium constants, K_{eq}, were evaluated using a previously reported procedure.⁴⁴ The equation for the evaluation of the K_{eq} is as follows:

$$1/K_{eq} = [\text{base}] \{ [\text{corrole}] L(\epsilon_c - \epsilon_{ca}) / (A_n - A_0) - 1 \}$$

where ϵ_c and ϵ_{ca} are the molar extinction coefficients of the free-base corrole and corrole-anion complex, respectively. A_0 and A_n are the absorbance values in the absence and in the presence of added anion at a particular wavelength. L is the path length of the cell employed. A plot of $[\text{anion}]^2$ versus $[\text{anion}]^2/A_n - A_0$ yielded a straight line. Using the above equation, the K_{eq} can be evaluated by taking the negative of the 1/intercept. The stoichiometry of binding was analysed by the Hill method.⁴⁵ A Hill plot was constructed by plotting $\ln[(A_0 - A_n)/(A_n - A_f)]$ against $\ln[\text{anion}]$, where A_0 and A_n are the absorbance values of the corrole employed and the corrole-anion complex, respectively, at a given concentration of the anion added. Note that A_f denotes the absorbance of the completely bound corrole-anion complex at a particular wavelength. The slope of the line was found to be two, which indicates a 1:2 stoichiometry between the corrole and the added anion. The above-mentioned method was employed for protonation and deprotonation studies.

Synthesis of (4-diethoxyphosphoryl)benzaldehyde⁴⁶

1 g of 4-bromobenzaldehyde (5.40 mmol) was taken in a 100 mL two-necked RB flask. To this solution, dry toluene (8 mL), dry triethylamine (8 mL) and diethyl phosphite (0.773 mL, 6 mmol) were added and purged with Ar gas for 2 minutes. Finally, Pd(PPh₃)₄ (0.31 g, 0.27 mmol) was added and the reaction mixture heated to 90 °C for 24 h under argon atmosphere. The reaction mixture was cooled to room temperature and the solvent mixture evaporated to dryness under vacuum, redissolved in CHCl₃ (70 mL), washed with distilled water (3 × 100 mL), followed by brine solution (100 mL), and finally dried over sodium sulphate. The crude product was purified on a silica column using CHCl₃-EtOAc (7:3, v/v) as the eluent. The yield of (4-diethoxyphosphoryl)benzaldehyde was found to be 0.8 g (61%).

¹H NMR (CDCl₃): δ (ppm) 10.05 (s, 1H, CHO), 7.62 (m, 2H, *o*-ph-H), 7.42 (td, $J = 8$ Hz, $J = 2.5$ Hz, 2H, *m*-ph-H), 4.12 (m, 4H, -OCH₂), 1.30 (t, $J = 7.1$ Hz, 6H, -CH₃).

5,10,15-Tris(4'-diethoxyphosphorylphenyl)corrole (H₃TPPC) [2]. (4-Diethoxyphosphoryl)benzaldehyde (1 g, 4.13 mmol) and pyrrole (0.570 mL, 8.26 mmol) were dissolved in 400 mL of a water and MeOH (1:1, v/v) mixture. Subsequently, 3.5 mL of conc. HCl (36%) was added dropwise and stirred for 3 h at room temperature. The reaction mixture was extracted with 100 mL of CHCl₃, washed twice with water (2 × 100 mL), dried over Na₂SO₄, and diluted with CHCl₃ to 270 mL. To this solu-

tion, *p*-chloranil (1 g, 1 mmol) was added and then refluxed for 1 h. The crude product was purified on a silica column using 3% MeOH in CHCl₃ as the eluent. Yield of **2** was found to be 10% (0.130 g, 0.139 mmol).

UV/Vis (CH₂Cl₂): λ_{max} (nm) (ε × 10⁻³ L mol⁻¹ cm⁻¹) 419 (66.0), 575 (11.2), 617 (8.1), 647 (6.6). ¹H NMR in CDCl₃ (500 MHz): δ (ppm) 9.04 (d, 2H, *J* = 4.15 Hz, β-pyrrole-H), 8.89 (d, 2H, *J* = 4.7 Hz, β-pyrrole-H), 8.63 (d, 2H, *J* = 4.1 Hz, β-pyrrole-H), 8.56 (d, 2H, *J* = 4.7 Hz, β-pyrrole-H), 8.46–8.50 (m, 4H, *meso-o*-phenyl-H), 8.18–8.32 (m, 8H, *meso-o* and *m*-phenyl-H), 4.30–4.42 (m, 12H, -OCH₂), 1.51 (t, 18H, *J* = 6.47 Hz, -CH₃) ESI-MS (*m/z*): found 971.272 [M + Cl⁻], calcd 971.268. Anal. calcd for C₄₉H₅₃N₄O₉P₃: C, 62.95; H, 5.71; N, 5.99%. Found: C, 62.70; H, 5.95; N, 6.15%.

Preparation of the Cu(III) and Ag(III) corrole complexes

Free-base corrole (0.050 g, 0.0535 mmol) was dissolved in 30 mL of CHCl₃. To this solution, 10 equiv. of copper(II) acetate monohydrate or silver(I) acetate in 8 mL of MeOH was added and stirred at room temperature for 1 h. Then, the reaction mixture was evaporated to dryness, redissolved in the minimum amount of CHCl₃ (15 mL) and washed with distilled water (50 mL). The organic layer was dried over Na₂SO₄ and purified on silica column using 1% MeOH in CHCl₃ as the eluent. The yields of **2a**, **2b**, **3a** and **3b** are reported below along with their characterisation data.

5,10,15-Tris(4'-diethoxyphosphorylphenyl)corrolato Cu(III) [2a]. UV/Vis (CH₂Cl₂): λ_{max} (nm) (ε × 10⁻³ L mol⁻¹ cm⁻¹) 412 (54.9), 536 (4.2), 617 (2.9). ¹H NMR in CDCl₃ (500 MHz): δ (ppm) 7.90–7.96 (m, 8H, *meso-o*, *m* and *p*-phenyl-H), 7.84–7.86 (m, 4H, *meso-o*-phenyl-H), 7.74–7.75 (m, 2H, β-pyrrole-H), 7.61 (d, 2H, *J* = 3.8 Hz, β-pyrrole-H), 7.32 (d, 2H, *J* = 3.9 Hz, β-pyrrole-H), 7.20 (d, 2H, *J* = 4.4 Hz, β-pyrrole-H), 4.28–4.12 (m, 12H, -OCH₂), 1.41 (at, 18H, *J* = 4.7 Hz, -CH₃) MALDI-TOF-MS (*m/z*): 995.420 [M]⁺ (calcd, 995.425). The yield of **2a** was found to be 56% (30 mg, 0.03 mmol).

5,10,15-Tris(4'-diethoxyphosphorylphenyl)corrolato Ag(III) [2b]. UV/Vis (CH₂Cl₂): λ_{max} (nm) (ε × 10⁻³ L mol⁻¹ cm⁻¹) 429 (57.5), 561 (8.3), 583 (15.1). ¹H NMR in CDCl₃ (500 MHz): δ (ppm) 9.26 (d, 2H, *J* = 4.0 Hz, β-pyrrole-H), 8.99 (d, 2H, *J* = 4.5 Hz, β-pyrrole-H), 8.79 (d, 2H, *J* = 4.0 Hz, β-pyrrole-H), 8.75 (d, 2H, *J* = 5.0 Hz, β-pyrrole-H), 8.41–8.44 (m, 4H, *meso-o*-phenyl-H), 8.33–8.35 (m, 2H, *meso-o*-phenyl-H), 8.29–8.25 (m, 6H, *meso-m*-phenyl-H), 4.43–4.36 (m, 12H, -OCH₂), 1.52 (t, *J* = 6.5 Hz, 18H, -CH₃) MALDI-TOF-MS (*m/z*): 1057.740 [M·H₂O]⁺ (calcd, 1057.757). The yield of **2b** was found to be 45% (25 mg, 0.024 mmol).

5,10,15-Tris(4'-carbomethoxyphenyl)corrolato Cu(III) [3a]. UV/Vis (CH₂Cl₂): λ_{max} (nm) (ε × 10⁻³ L mol⁻¹ cm⁻¹) 414 (47.8), 541 (3.4), 626 (2.3). ¹H NMR in CDCl₃ (500 MHz): δ (ppm) 8.20 (d, 4H, *J* = 7.5 Hz, *meso-o*-phenyl-H), 8.17 (d, 2H, *J* = 8.0 Hz, *meso-o*-phenyl-H), 7.96 (d, 2H, *J* = 3.2 Hz, β-pyrrole-H), 7.84 (d, 4H, *J* = 8.1 Hz, *meso-m*-phenyl-H), 7.74 (d, 2H, *J* = 8.1 Hz, *meso-m*-phenyl-H), 7.62 (d, 2H, *J* = 4.3 Hz, β-pyrrole-H), 7.34 (d, 2H, *J* = 4.3 Hz, β-pyrrole-H), 7.21 (d, 2H, *J* = 4.6 Hz, β-pyrrole-H), 4.02 (s, 6H, -OCH₃), 4.01 (s, 3H, -OCH₃). MALDI-TOF-MS

(*m/z*): 761.348 [M]⁺ (calcd, 761.273). The yield of **3a** was found to be 66% (36 mg, 0.047 mmol).

5,10,15-Tris(4'-carboxymethylphenyl)corrolato Ag(III) [3b]. UV/Vis (CH₂Cl₂): λ_{max} (nm) (ε × 10⁻³ L mol⁻¹ cm⁻¹) 428 (64.5), 527 (4.5), 584 (17.4). ¹H NMR in CDCl₃ (500 MHz): δ (ppm) 9.07 (d, 2H, *J* = 4.3 Hz, β-pyrrole-H), 8.92 (d, 2H, *J* = 4.7 Hz, β-pyrrole-H), 8.68 (d, 2H, *J* = 4.5 Hz, β-pyrrole-H), 8.66 (d, 2H, *J* = 4.5 Hz, β-pyrrole-H), 8.49 (d, 4H, *J* = 8.1 Hz, *meso-o*-phenyl-H), 8.45 (d, 2H, *J* = 8.1 Hz, *meso-o*-phenyl-H), 8.34 (d, 4H, *J* = 8.1 Hz, *meso-m*-phenyl-H), 8.23 (d, *J* = 8.1 Hz, 2H, *meso-m*-phenyl-H), 4.12 (s, 6H, -OCH₃), 4.11 (s, 3H, -OCH₃). MALDI-TOF-MS (*m/z*): 805.373 [M]⁺ (calcd, 805.589). The yield of **3b** was found to be 56% (32 mg, 0.039 mmol).

Results and discussion

Synthesis and characterization

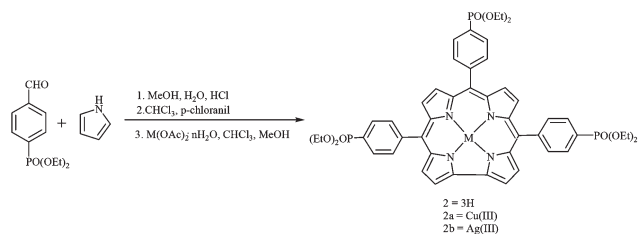
We have synthesized different free-base corroles (**1**–**3**) and their Cu(III) and Ag(III) complexes as shown in Chart 1. **1** and **3** were synthesized according to the procedure described by Gryko in a H₂O–MeOH mixture.^{4a} Initially, we tried to synthesize 5,10,15-tris(4'-diethoxyphosphorylphenyl)corrole *via* Pd-catalysed coupling reaction using 5,10,15-tris(4'-bromophenyl)corrole and diethylphosphite by refluxing in ethanol under an argon atmosphere as reported in the literature for the synthesis of phosphorylporphyrins.²⁹ Unfortunately, the reaction yielded an inseparable mixture of products in a very low yield (<0.5%). Alternatively, we synthesized 4-diethoxyphosphorylbenzaldehyde⁴⁶ and then condensed it with pyrrole in a water-methanol mixture^{4a} and the yield was found to be 10% (Scheme 1).

The Ag(III) and Cu(III) metal complexes were prepared by reacting the free-base corroles and the corresponding metal acetates in a CHCl₃–methanol mixture as shown in Scheme 1. All the synthesized corroles were characterized by UV-Visible, fluorescence, ¹H NMR and mass spectroscopic techniques.

The UV-visible spectral features of **2** and **2a–b** in CH₂Cl₂ are shown in Fig. 1a. Table 1 shows the optical absorption spectral data of the corroles synthesized. Moreover, the electronic absorption spectra of **3** and **3a–b** are shown in the ESI



Chart 1 Molecular structures of the corroles synthesized.



Scheme 1 Synthesis of triphosphorylphenylcorrole (**2**) and its metal complexes (**2a** and **2b**).

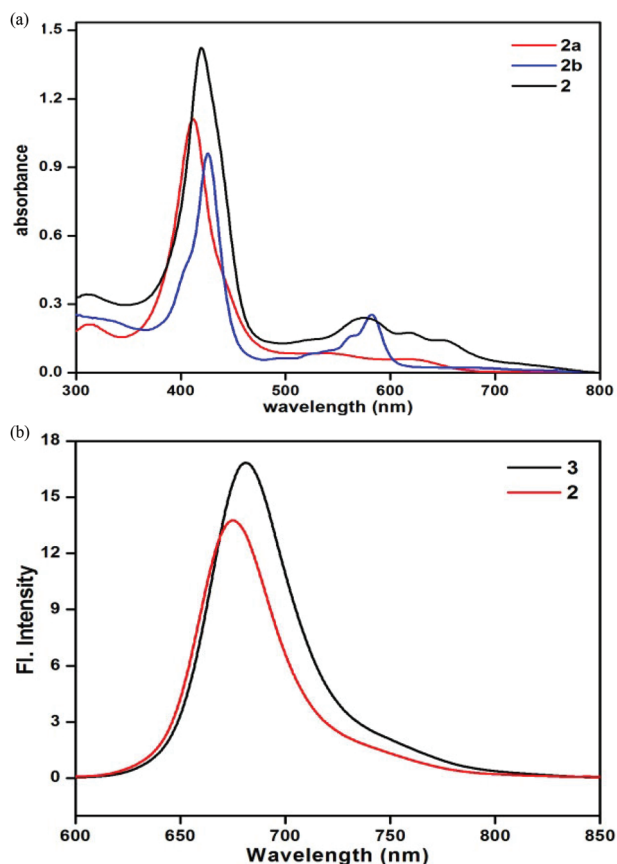


Fig. 1 (a) UV-Visible spectra of **2** and **2a–b** in CH_2Cl_2 . (b) Fluorescence spectra of **2** and **3** in CH_2Cl_2 .

Table 1 Optical absorption spectral data of compounds **1–3** and their metal complexes (λ_{max} (nm) ($\epsilon \times 10^{-3} \text{ L mol}^{-1} \text{ cm}^{-1}$)) in CH_2Cl_2

| Corrole | B band (nm) | Q bands (nm) |
|-----------|-------------|----------------------------------|
| 2 | 419 (66.0) | 575 (11.2), 617 (8.1), 647 (6.6) |
| 2a | 412 (54.9) | 536 (4.1), 617 (2.9) |
| 2b | 429 (57.5) | 561 (8.3), 583 (15.1) |
| 3 | 424 (52.5) | 579 (9.3), 622 (6.6), 653 (4.9) |
| 3a | 414 (47.8) | 542 (3.4), 621 (2.3) |
| 3b | 428 (64.5) | 526 (4.5), 584 (17.4) |

(Fig. S1†). **2** shows a Soret band at 419 nm and three Q bands at 575, 617 and 647 nm, which are marginally red shifted compared to **1** and 5 nm blue-shifted than **3**. Fig. 1b shows the

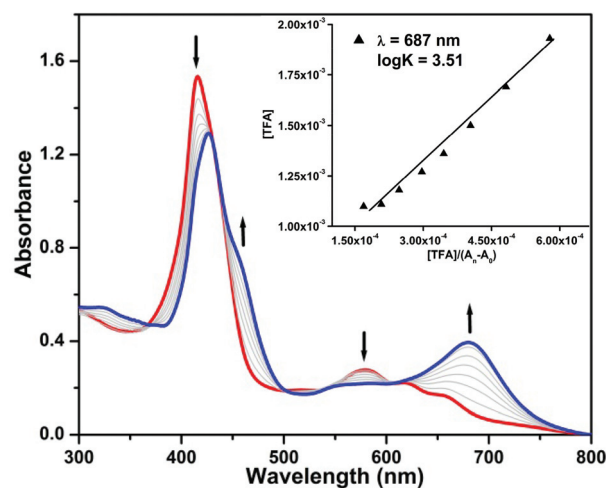


Fig. 2 UV-Visible spectral titration of **2** ($2.13 \times 10^{-5} \text{ M}$) with μM concentration of TFA in acetonitrile. The inset shows a plot between $[\text{TFA}]$ and $[\text{TFA}]/(A_n - A_0)$.

emission spectra of **2** and **3** in CH_2Cl_2 showing maxima at 678 and 686 nm, respectively. **2** exhibited a 7 nm red shift and 8 nm blue-shift as compared to **1** and **3**, respectively.

^1H NMR spectrum of **2** shows the characteristic four doublets corresponding to β -protons of the corrole macrocycle. A multiplet at 4.30–4.42 ppm (12 H) and a triplet at 1.51 ppm (18 H) confirm the diethoxyphosphoryl group at the *meso*-phenyl position of the corrole. ^1H NMR signals of **2b** showed a downfield shift (0.2–0.3 ppm) than **2** and **2a**, possibly due to the enhanced planarity in the Ag corrole complexes.⁴⁷ The ^1H NMR spectra of **2**, **2a**, **2b** and **3b** are shown in the ESI (Fig. S2–S5†). Aggregation behaviour of **2** and **3** were studied using a UV-Visible spectrophotometer at various concentrations (0.53 – $1.59 \times 10^{-5} \text{ M}$) in CH_2Cl_2 . These corroles did not show any considerable changes, which indicates that **2** and **3** do not aggregate in CH_2Cl_2 at a concentration of 10^{-5} M , whereas the broad peaks observed in the ^1H NMR spectra of **2** and **3** at $\sim 0.015 \text{ M}$ in CDCl_3 indicates the aggregation behaviour of these corroles at higher concentrations. The MALDI-TOF mass spectra of **2a**, **2b**, **3a** and **3b** are shown in the ESI (Fig. S6–S9†) and the experimental mass values are in accordance with the calculated mass values for $[\text{M}^+]$.

Protonation studies

Protonation studies of the free-base corroles (**1–3**) were studied in CH_3CN using trifluoroacetic acid (TFA) as the titrating agent. Fig. 2 shows the UV-Visible spectral changes of **2** with an increase in the concentration of TFA. The absorbance at 421 nm for **2** had concomitant decrement and a new shoulder was observed at 429 nm with a 8 nm red-shift. Similarly, **2** showed a concomitant decrement in the absorbance at 582 nm and a rising new band at 680 nm accompanied with a red-shift of 22 nm in the Q band as shown in Fig. 2. In all cases, we obtained a monoprotinated corrole species, which was further confirmed by the Hill plot showing a slope value

of **1** (Fig. S10a in the ESI†). All the monocationic corroles (Scheme 1) exhibited a stable aromatic nature as confirmed by their UV-Visible spectral features. A representative plot for the evaluation of K_{eq} for the protonation of **2** is shown as an inset in Fig. 2. Moreover, a similar behaviour was observed for **1** and **3** as shown in Fig. S11 in the ESI† Table 2 lists the protonation constants for **1–3** in CH_3CN . The highest $\log K$ was observed for **1** (4.93) and lowest for **2** (3.75), which suggests that the electron-withdrawing nature of the phosphoryl groups makes it difficult to protonate the inner core nitrogen of corrole **2**. Similar results were obtained for **3** as compared to **1**. The protonation constants ($\log K$) follow the trend expected: **1** > **3** > **2**.

Deprotonation studies

A UV-Visible titration method was employed to determine the deprotonation constants of **1–3** in CH_3CN using tetrabutylammonium hydroxide (TBAOH) as a base and the spectral changes of **2** during the course of titration shown in Fig. 3. The absorbance decreased at 421 nm with the emergence of a new B band at 442 nm accompanied by a 21 nm red-shift. Similar behaviour was observed for the Q-bands (decrement in the absorbance at 583 nm and a concomitant increase in absorbance at 646 nm) as shown in Fig. 3. The inset shows a straight line between $[\text{TBAOH}]^2/A_0 - A_n$ versus $[\text{TBAOH}]^2$ from which the β_2 value was calculated for the deprotonation of **2**. The Hill plot refers to a 1:2 stoichiometry or two proton abstraction by the base (TBAOH) as shown in Fig. S10b (ESI†)

Table 2 Protonation and deprotonation constants of **1–3** in CH_3CN

| Corrole | TFA | | | TBAOH | | |
|----------|--------------------|----------|-----|--------------------|----------------|-----|
| | K | $\log K$ | n | β_2 | $\log \beta_2$ | n |
| 1 | 8.52×10^4 | 4.93 | 1 | 5.76×10^9 | 9.76 | 2 |
| 2 | 0.32×10^4 | 3.51 | 1 | 1.89×10^9 | 9.27 | 2 |
| 3 | 0.94×10^4 | 3.97 | 1 | 1.91×10^9 | 9.28 | 2 |

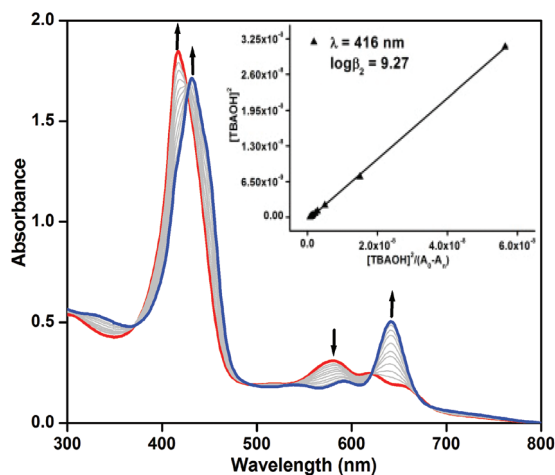


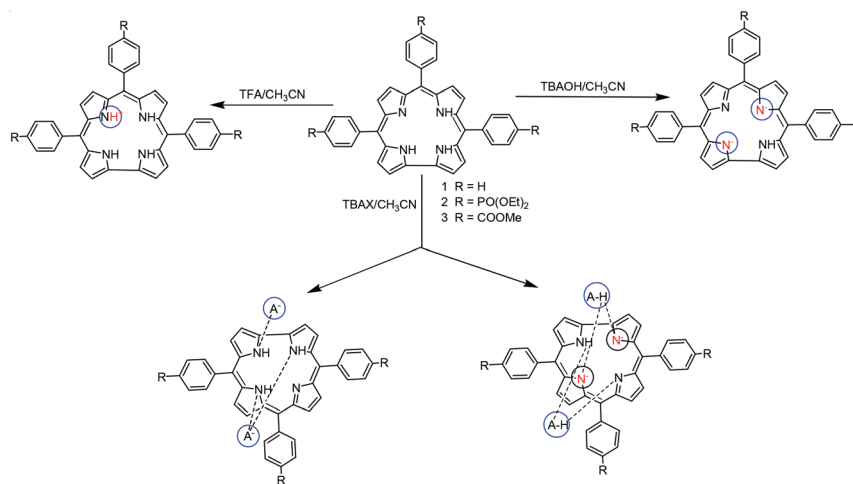
Fig. 3 UV-Visible spectral changes in **2** (2.59×10^{-5} M) during the addition of TBAOH in acetonitrile (the inset shows a plot between $[\text{TBAOH}]^2$ and $[\text{TBAOH}]^2/(A_0 - A_n)$).

and Scheme 2. Deprotonation spectral changes of **3** are shown in Fig. S12 in the ESI† The deprotonation constants of **1–3** are summarized in Table 2. The $\log \beta_2$ value of **2** (9.27) is marginally less than the free base β -octaethylcorrole (9.50) and close to tris(*p*-methylphenyl)corrole (9.2).³⁶ This suggests that the acidity of the imino protons of **2** and **3** are comparable to that of **1**, which is different from the expected trend.

Anion detection

Anion detection by **1–3** was studied in CH_3CN with various spherical halide ions such as F^- , Cl^- , Br^- and I^- and bulky anions such as CH_3COO^- , H_2PO_4^- , HSO_4^- , PF_6^- and ClO_4^- using a UV-Visible spectrophotometer with the addition of an aliquot of anionic TBA salts. The free-base corroles (**1–3**) selectively bind with F^- , CH_3COO^- and H_2PO_4^- ions and show a considerable red-shift (10–15 nm) in the UV-Visible spectra as shown in Fig. 4 and S13a (ESI†), whereas no shifts were observed for other anions. There are two possibilities of corrole and anion interaction: (i) anions may have strong hydrogen bonding with the NH moieties in the corrole core or (ii) these basic anions can abstract the acidic proton of NH group, a process called anion induced deprotonation. The UV-visible spectral changes of receptor **2** with different anions were the same as that of TBAOH (Fig. 4). These results indicate that the spectral changes were most probably due to the deprotonation of the NH moiety by the basic anions (F^- , CH_3COO^- and H_2PO_4^-) and not through hydrogen bonding. The spectrophotometric titration of **2** with fluoride ions is shown in Fig. 5. As we increased the concentration of F^- ions, a decrement in the absorbance was observed at 417 nm and 581 nm and a concomitant increment in the absorbance at 432 nm and 642 nm, respectively with the isosbestic points at 425 nm and 618 nm. The equilibrium constant for F^- ion binding was calculated using a plot of $[\text{anion}]^2$ versus $[\text{anion}]^2/A_n - A_0$ as shown in the inset of Fig. 5. The Hill plot (Fig. S13b in the ESI†) shows a straight line between $\log[\text{F}^-]$ and $\log(A_0 - A_n/A_f - A_n)$ with a slope value of 2, which indicates a 1:2 (corrole-to-anion) stoichiometry as shown in Scheme 2. A similar behavior was observed for **3** as shown in Fig. S14 in the ESI† Similar spectral changes were obtained for CH_3COO^- and H_2PO_4^- with **1–3** (Fig. S15–S16 in the ESI†). The equilibrium constants of **1–3** with different anions are summarized in Table 3. The F^- , CH_3COO^- and H_2PO_4^- induced deprotonation is fully reversible as shown upon the addition of CH_3OH . The addition of a polar protic solvent such as CH_3OH results in a gradual decrease in the absorbance as reflected in the UV-Visible spectral studies (see Fig. S17 in the ESI†). This is possibly due to competition between the protic solvent versus the anions (F^- , CH_3COO^- and H_2PO_4^-) with NH moiety. Moreover, the presence of a high amount of protic solvent disfavors the formation of the deprotonated receptor **2**.

2 and **3** have shown higher equilibrium constants with F^- ions (4.7×10^3 fold higher for **2** and 9.7×10^3 fold higher for **3**) as compared to that of **1**. The electron-withdrawing nature of diethoxyphosphoryl and carbomethoxy groups make corroles **2** and **3** more acidic, which is responsible for the deprotonation



Scheme 2 Schematic representation of protonation, deprotonation and anion binding with 1–3.

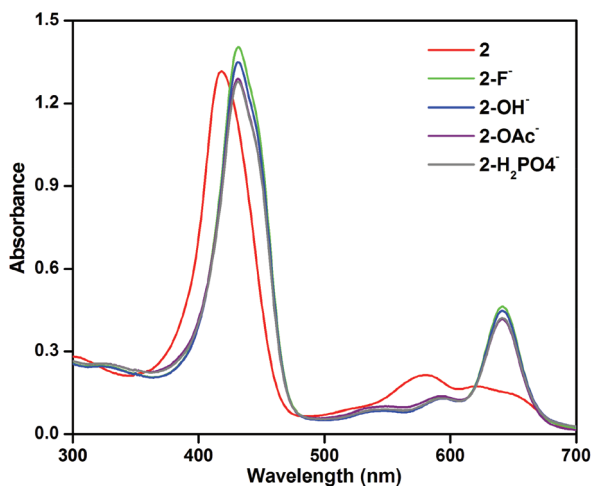


Fig. 4 Absorption spectral changes of 2 with μM quantities of base and anions.

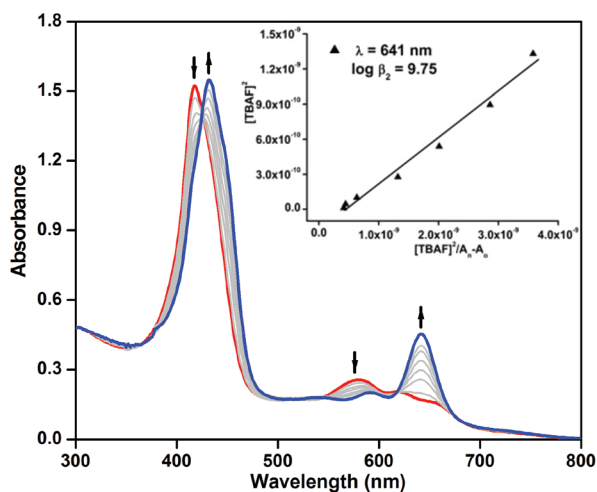


Fig. 5 UV-Visible titration of 2 (2.13×10^{-5} M) with TBAF (the inset shows a plot between $[\text{TBAF}]^2$ and $[\text{TBAF}]^2/(A_0 - A_n)$).

Table 3 Equilibrium constants^a of 1–3 upon the addition of μM quantities of anions in CH_3CN

| Compound | Anion | $\text{Log } \beta_2$ | A : L | LOD (μM) | LOQ (μM) |
|----------|---------------------------|-----------------------|-------|-----------------------|-----------------------|
| 1 | F^- | 6.06 | 1 : 1 | 0.50 | 2.43 |
| | CH_3COO^- | 10.53 | 2 : 1 | 0.18 | 6.48 |
| | H_2PO_4^- | 9.39 | 2 : 1 | 0.17 | 6.90 |
| 2 | F^- | 9.74 | 2 : 1 | 0.06 | 0.17 |
| | CH_3COO^- | 10.80 | 2 : 1 | 0.05 | 0.14 |
| | H_2PO_4^- | 10.27 | 2 : 1 | 0.05 | 0.14 |
| 3 | F^- | 10.05 | 2 : 1 | 0.06 | 0.19 |
| | CH_3COO^- | 9.63 | 2 : 1 | 0.04 | 0.12 |
| | H_2PO_4^- | 9.50 | 2 : 1 | 0.04 | 0.11 |

^a Within the error ± 0.14 .

of the inner core NH protons by basic anions as compared to 1. No changes were observed for 1–3 in the presence of Cl^- , Br^- , I^- , HSO_4^- , PF_6^- and ClO_4^- . This indicates that the receptor provides selectivity towards F^- , CH_3COO^- and H_2PO_4^- , which is solely based upon its deprotonation and is related to the following factors: (a) the intrinsic acidity of the receptor, (b) the basicity of the anion and (c) the polarity of the solvent.⁴⁸ The imino protons of the free-base corroles (2 and 3) are highly acidic in nature; hence, they are sensitive for basic anions such as F^- , CH_3COO^- and H_2PO_4^- ions. The small ionic size (1.3 Å) and the high electronegativity (4.1) of fluoride ions are responsible for the easy deprotonation of the NH group as compared to other anions. Moreover, the size of the corrole core (2.50 Å) is compatible with the fluoride ion size, which is responsible for the higher equilibrium constants observed.

The limit of detection (LOD) and limit of quantification (LOQ) for F^- , CH_3COO^- and H_2PO_4^- were calculated in the presence of 1–3 in CH_3CN . 2 shows more sensitivity towards F^- ions, the LOD for 2 was found to be 0.06 μM and the LOQ was found to be 0.17 μM . 3 shows higher sensitivity towards the basic anions CH_3COO^- and H_2PO_4^- with a very low detection limit of 0.04 μM . These results suggest that 2 and 3 are

very much sensitive for anion detection as compared to other reported corroles.^{20a}

Electrochemistry

To probe the influence of the *meso*-phenyl substituents on the π -electronic properties of the corrole ring system, the electrochemical redox behaviours of these corroles were studied by cyclic voltammetric analysis. **1–3** showed two reversible oxidations and one irreversible reduction as shown in Fig. S18 in the ESI.† **2** and **3** exhibited an anodic shift in their first oxidation (~ 120 mV) and reduction (160–400 mV) potentials as compared to **1**. Since the anionic radicals of **1–3** formed after electrochemical reduction are unstable and undergo disproportionation we used their metal complexes to probe further. The CVs of the Ag(III) and Cu(III) complexes of **1–3** are shown in Fig. 6. **1b** shows three oxidations and two reductions as reported in the literature,⁴⁷ whereas **2b** and **3b** show two ring centred oxidations and one metal centred reduction (Table 4). The first oxidation potentials of **2a–b** and **3a–b** are more anodically shifted (~ 250 mV) as compared to **1a–b**. The metal centred reductions of **2a** and **3a** are anodically shifted (~ 100 – 150 mV) as compared to **1a**. The anodic shift of redox potentials is ascribed to the strong electron-withdrawing nature of the diethoxyphosphoryl and carbomethoxy groups present.

The higher reduction potentials of the Ag(III) corroles as compared to the Cu(III) corroles is due to the more electropositive nature of silver metal. For the Hammett equation $E_{1/2} = 3\sigma_p$, the plot of first ring oxidation and metal centred reduction versus the Hammett parameter (σ_p) of the substituents was examined to delineate the role of the substituents on the corrole π -system and exhibited a linear trend, as shown in Fig. 7. The reaction constant, ρ , for the first oxidation versus σ_p was found to be higher (195 mV) for the Ag corroles relative to that of the Cu corroles (165 mV), which indicates the higher reactivity of the Ag corrole towards oxidation. The reaction constant obtained from the plot of reduction potential versus σ_p was found to be higher for the Cu corroles (91 mV) as com-

Table 4 Electrochemical redox data for compounds **1–3** and their metal complexes in CH_2Cl_2

| Corrole | 3σ | Oxidation | | | Reduction | |
|-----------|-----------|-----------|------|------|-----------|-------|
| | | I | II | III | I | II |
| 1a | 0 | 648 | 1420 | — | –223 | — |
| 2a | 1.59 | 904 | 1385 | — | –76 | — |
| 3a | 1.35 | 882 | — | — | –105 | — |
| 1b | 0 | 580 | 744 | 1239 | –836 | –1017 |
| 2b | 1.59 | 884 | 1372 | — | –752 | — |
| 3b | 1.35 | 856 | 1295 | — | –800 | — |

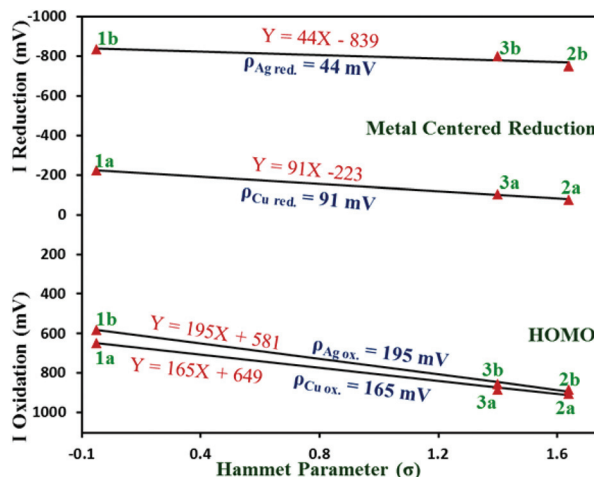


Fig. 7 A plot of Hammett parameter (3σ) versus the first ring oxidation and the metal centred reduction of the Cu(III) and Ag(III) complexes derived from **1–3**.

pared to the Ag corroles (44 mV), which indicates a higher tendency towards reduction for the Cu corroles. These results clearly indicate that the diethoxyphosphoryl and carbomethoxy corroles are electron deficient in nature; therefore, they show highest equilibrium constant towards the basic anions.

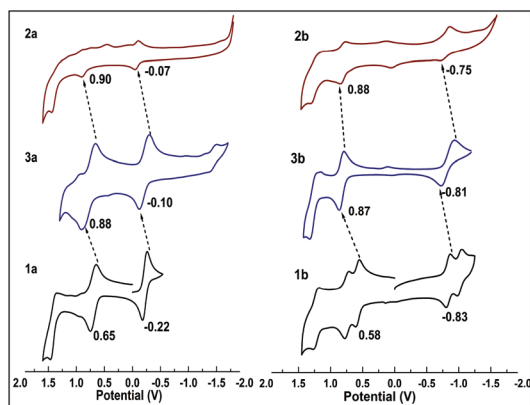


Fig. 6 Cyclic Voltammograms of **1a–3b** in CH_2Cl_2 containing 0.1 M TBAP (with a scan rate of 100 mV s^{-1}). A GC working electrode, Ag/AgCl reference electrode and Pt wire counter electrode were used.

Conclusion

We have synthesized a new family of electron deficient corroles and characterized them using spectroscopic techniques and electrochemical studies. **2** and **3** exhibited red-shifted absorption spectra and a downfield shift in their ^1H NMR spectra as compared to **1**. The protonation constant of **2** is ~ 30 fold lower as compared to **1**, reflecting the electron-withdrawing nature of the diethoxyphosphoryl groups. **2** and **3** have shown higher equilibrium constants with F^- ions (4.7×10^3 fold higher for **2** and 9.7×10^3 fold higher for **3**) as compared to **1** and are able to detect $0.06 \mu\text{M}$ of F^- ions. **2** was also found to be more sensitive towards CH_3COO^- and H_2PO_4^- ions, and it allowed the detection of $0.05 \mu\text{M}$ of these anions with a LOQ of $0.14 \mu\text{M}$. Tricarbomethoxyphenyl and triphosphorylphenyl substituted

metallocorroles exhibited an anodic shift of ~250 mV in the oxidation and ~100–150 mV in their metal centered reduction as compared to **1** due to the electron-withdrawing nature of the substituents. The linear trend in the Hammett plot also substantiates the effect of the substituents on the corrole π -system. These results indicate that the electron-deficient corroles can be utilized as efficient basic anion detectors.

Acknowledgements

We are grateful for the financial support provided by the Council of Scientific and Industrial Research (01(2694)/12/EMR-II), Science and Engineering Research Board (SB/FT/CS-015/2012) and Board of Research in Nuclear Sciences (2012/37C/61BRNS/253). PY thanks CSIR for the Junior Research Fellowship (JRF).

References

- 1 A. W. Johnson and I. T. Kay, *J. Chem. Soc.*, 1965, 1620.
- 2 (a) R. Paolesse, L. Jaquinod, D. J. Nurco, S. Mini, F. Sagone, T. Boschi and K. M. Smith, *Chem. Commun.*, 1999, 1307–1308; (b) R. Paolesse, S. Nardis, F. Sagone and R. G. Khoury, *J. Org. Chem.*, 2001, **66**, 550–556.
- 3 (a) Z. Gross, N. Galili, L. Simkhovich, I. Saltsman, M. Botoshansky, D. Blaser, R. Boese and I. Goldberg, *Org. Lett.*, 1999, **1**, 599–602; (b) Z. Gross, N. Galili and I. Saltsman, *Angew. Chem., Int. Ed.*, 1999, **38**, 1427–1429.
- 4 (a) B. Koszarna and D. T. Gryko, *J. Org. Chem.*, 2006, **71**, 3707–3717; (b) C. Capar, L. K. Hansen, J. Conradie and A. Ghosh, *J. Porphyrins Phthalocyanines*, 2010, **14**, 509–512; (c) K. E. Thomas, I. H. Wasbotten and A. Ghosh, *Inorg. Chem.*, 2008, **47**, 10469–10478; (d) A. Ghosh, *Angew. Chem., Int. Ed.*, 2004, **43**, 1918–1931; (e) E. Steene, A. Dey and A. Ghosh, *J. Am. Chem. Soc.*, 2003, **125**, 16300–16309.
- 5 C. Erlen, S. Will and K. M. Kadish, in *The Porphyrin Handbook*, ed. K. M. Kadish, K. M. Smith and R. Guilard, Academic Press, New York, 2000, vol. 2, pp. 233–300.
- 6 J. Bendix, I. J. Dmochowski, H. B. Gray, A. Mahammed, L. Simkhovich and Z. Gross, *Angew. Chem., Int. Ed.*, 2000, **39**, 4048–4051.
- 7 A. Mahammed and Z. Gross, *J. Inorg. Biochem.*, 2002, **88**, 305–309.
- 8 K. Sorasaene, P. Taqavi, L. M. Heling, H. B. Gray, E. Tkachenko, A. Mahammed and Z. Gross, *J. Porphyrins Phthalocyanines*, 2007, **11**, 189–197.
- 9 S. Nardis, D. Monti and R. Paolesse, *Mini-Rev. Org. Chem.*, 2005, **2**, 355–372.
- 10 Z. Gross, *J. Biol. Inorg. Chem.*, 2001, **6**, 733–738.
- 11 Z. Gross and H. B. Gray, *Comments Inorg. Chem.*, 2006, **27**, 61–72.
- 12 S. H. Kim, H. Park, M. S. Seo, M. Kubo, T. Ogura, J. Klajn, D. T. Gryko, J. S. Valentine and W. Nam, *J. Am. Chem. Soc.*, 2010, **132**, 14030–14032.
- 13 H. Y. Liu, M. H. R. Mahmood, S. X. Qiu and C. K. Chang, *Coord. Chem. Rev.*, 2013, **257**, 1306–1333.
- 14 Y. Han, Y. M. Lee, M. Mariappan, S. Fukuzumi and W. Nam, *Chem. Commun.*, 2010, **46**, 8160–8162.
- 15 (a) Z. Gross, L. Simkhovich and N. Galili, *Chem. Commun.*, 1999, 599–600; (b) K. M. Kadish, L. Fremond, F. Burdet, J.-M. Barbe, C. P. Gros and R. Guilard, *J. Inorg. Biochem.*, 2006, **100**, 858–868.
- 16 (a) G. Golubkov, J. Bendix, H. B. Gray, A. Mahammed, I. Goldberg, A. J. DiBilio and Z. Gross, *Angew. Chem., Int. Ed.*, 2001, **40**, 2132–2134; (b) H. Y. Liu, T. S. Lai, L. L. Yeung and C. K. Chang, *Org. Lett.*, 2003, **5**, 617–620.
- 17 I. Luobeznova, M. Raizman, I. Goldberg and Z. Gross, *Inorg. Chem.*, 2006, **45**, 386–394.
- 18 G. Golubkov and Z. Gross, *J. Am. Chem. Soc.*, 2005, **127**, 3258–3259.
- 19 R. Paolesse, C. D. Natale, A. Macognano, F. Sagone, M. A. Scarselli, P. Chiaradia, V. I. Troitsky, T. S. Berzina and A. D'Amico, *Langmuir*, 1999, **15**, 1268–1274.
- 20 (a) C. I. M. Santos, E. Oliveira, J. F. B. Barata, M. A. F. Faustino, J. A. S. Cavaleiro, M. G. P. M. S. Neves and C. Lodeiro, *J. Mater. Chem.*, 2012, **22**, 13811–13819; (b) C. I. M. Santos, E. Oliveira, J. F. B. Barata, M. A. F. Faustino, J. A. S. Cavaleiro, M. G. P. M. S. Neves and C. Lodeiro, *Inorg. Chim. Acta*, 2014, **417**, 148–154.
- 21 R. Paolesse, F. Sagone, A. Macagnano, T. Boschi, L. Prodi, M. Montalti, N. Zaccheroni, F. Bolletta and K. M. Smith, *J. Porphyrins Phthalocyanines*, 1999, **3**, 364–370.
- 22 D. Walker, S. Chappel, A. Mahammed, J. J. Weaver, B. S. Brunschwig, J. R. Winkler, H. B. Gray, A. Zaban and Z. Gross, *J. Porphyrins Phthalocyanines*, 2006, **10**, 1259–1262.
- 23 K. Sudhakar, V. Velkannan and L. Giribabu, *Tetrahedron Lett.*, 2012, **53**, 991–993.
- 24 A. Haber, A. Mahammed, B. Fuhrman, N. Volkova, R. Coleman, T. Hayek, M. Aviram and Z. Gross, *Angew. Chem., Int. Ed.*, 2008, **47**, 7896–7900.
- 25 (a) A. Rebane, M. Drobizhev, N. S. Makarov, B. Koszarna, M. Tasior and D. T. Gryko, *Chem. Phys. Lett.*, 2008, **462**, 246–250; (b) P. T. Anusha, D. Swain, S. Hamad, L. Giribabu, T. S. Prashant, S. P. Tewari and S. V. Rao, *J. Phys. Chem. C*, 2012, **116**, 17828–17837.
- 26 S. Cho, J. M. Lim, S. Hiroto, P. Kim, H. Shinokubo, A. Osuka and D. Kim, *J. Am. Chem. Soc.*, 2009, **131**, 6412–6420.
- 27 X. Ying, X. Y. Long, M. H. R. Mahmood, Q. Y. Hu, H. Y. Liu and C. K. Chang, *J. Porphyrins Phthalocyanines*, 2012, **16**, 1276–1284.
- 28 K. E. Borbas, H. L. Kee, D. Holten and J. S. Lindsey, *Org. Biomol. Chem.*, 2008, **6**, 187–194.
- 29 K. M. Kadish, P. Chen, Y. Yu. Enakieva, S. E. Nefedov, Y. G. Gorbunovab, A. Y. Tsivadze, A. Bessmertnykh-Lemeune, C. Stern and R. Guilard, *J. Electroanal. Chem.*, 2011, **656**, 61–71.
- 30 A. A. Sinelshchikova, S. E. Nefedov, Y. Y. Enakieva, Y. G. Gorbunova, A. Y. Tsivadze, K. M. Kadish, P. Chen,

- A. Bessmertnykh-Lemeune, C. Stern and R. Guillard, *Inorg. Chem.*, 2013, **52**, 999–1008.
- 31 D. L. Officer, F. Lodato and K. W. Jolley, *Inorg. Chem.*, 2007, **46**, 4781–4783.
- 32 (a) Y. Fang, K. M. Kadish, P. Chen, Y. Gorbunova, Y. Enakieva, A. Tsivadze, A. Bessmertnykh-Lemeune and R. Guillard, *J. Porphyrins Phthalocyanines*, 2013, **17**, 1035–1045; (b) Z. Ou, J. Shen, J. Shao, M. Galezowski, D. T. Gryko and K. M. Kadish, *Inorg. Chem.*, 2007, **46**, 2775–2786; (c) J. Shen, Z. Ou, J. Shao, M. Galezowski, D. T. Gryko and K. M. Kadish, *J. Porphyrins Phthalocyanines*, 2007, **11**, 269–276; (d) Z. Ou, H. Suna, H. Zhua, Z. Daa and K. M. Kadish, *J. Porphyrins Phthalocyanines*, 2008, **12**, 1–10.
- 33 J. Shen, J. Shao, Z. Ou, B. Koszarna, D. T. Gryko and K. M. Kadish, *Inorg. Chem.*, 2006, **45**, 2251–2265.
- 34 J. P. Gisselbrecht, M. Gross, E. Vogel and S. Will, *J. Electroanal. Chem.*, 2001, **205**, 170–172.
- 35 A. Mahammed, J. J. Weaver, H. B. Gray, M. Abdelas and Z. Gross, *Tetrahedron Lett.*, 2003, **44**, 2077–2079.
- 36 R. Grigg, R. J. Hamilton, M. L. Jozefowicz, C. H. Rochester, R. J. Terrell and H. Wickwar, *J. Chem. Soc., Perkin Trans. 2*, 1973, 407–413.
- 37 M. J. Broadhurst, R. Grigg and G. Shelton, *J. Chem. Soc., Perkin Trans. 1*, 1972, 143–151.
- 38 P. E. Ellis, J. E. Linard, T. Szymanski, R. D. Jones, J. R. Budge and F. Basolo, *J. Am. Chem. Soc.*, 1980, **102**, 1889–1896.
- 39 C. Y. Li, X. B. Zhang, Z. X. Han, B. A. Kermack, L. Sun, G. L. Shena and R. Q. Yua, *Analyst*, 2006, **131**, 388–393.
- 40 Y. Zhang, M. X. Li, M. Y. Lu, R. H. Yang, F. Liu and K. A. Li, *J. Phys. Chem. A.*, 2005, **109**, 7442–7448.
- 41 (a) F. Zhi, X. Lu, J. Yang, X. Wang, H. Shang, S. Zhang and Z. Xue, *J. Phys. Chem. C*, 2009, **113**, 13166–13172; (b) P. Kubat, K. Lang and P. Anzenbacher, *Biochim. Biophys. Acta*, 2004, **1670**, 40–48.
- 42 J. M. M. Rodrigues, A. S. F. Farinha, F. P. V. Muteto, S. M. Woranovicz-Barreira, F. A. A. Paz, M. G. P. M. S. Neves, J. A. S. Cavaleiro, A. C. Tome, M. T. S. R. Gomes, J. L. Sessler and J. P. C. Tome, *Chem. Commun.*, 2014, **50**, 1359–1361.
- 43 V. M. Patel, J. A. Patel, S. S. Havele and S. R. Dhaneshwar, *Int. J. ChemTech Res.*, 2010, **2**, 756–761.
- 44 (a) J. P. Collman, J. I. Brauman, K. M. Doxsee, T. R. Halbert, S. E. Hayes and K. S. Suslick, *J. Am. Chem. Soc.*, 1978, **100**, 2761–2766; (b) K. S. Suslick, M. M. Fox and T. J. Reinert, *J. Am. Chem. Soc.*, 1984, **106**, 4522–4525.
- 45 (a) A. V. Hill, *J. Physiol.*, 1910, **40**, IV–VII; (b) C. A. Hunter, M. N. Meah and J. K. M. Sanders, *J. Am. Chem. Soc.*, 1990, **112**, 5773–5780.
- 46 S. K. Hau, Y. J. Cheng, H. L. Yip, Y. Zhang, H. Ma and A. K. Y. Jen, *Appl. Mater. Interfaces*, 2010, **2**, 1892–1902.
- 47 (a) A. Alemayehu, J. Conradie and A. Ghosh, *Eur. J. Inorg. Chem.*, 2011, 1857–1864; (b) K. E. Thomas, A. B. Alemayehu, J. Conradie, C. Beavers and A. Ghosh, *Inorg. Chem.*, 2011, **50**, 12844–12851.
- 48 A. K. Mahapatra, K. Maiti, P. Sahoo and P. K. Nandi, *J. Lumin.*, 2013, **143**, 349–354.